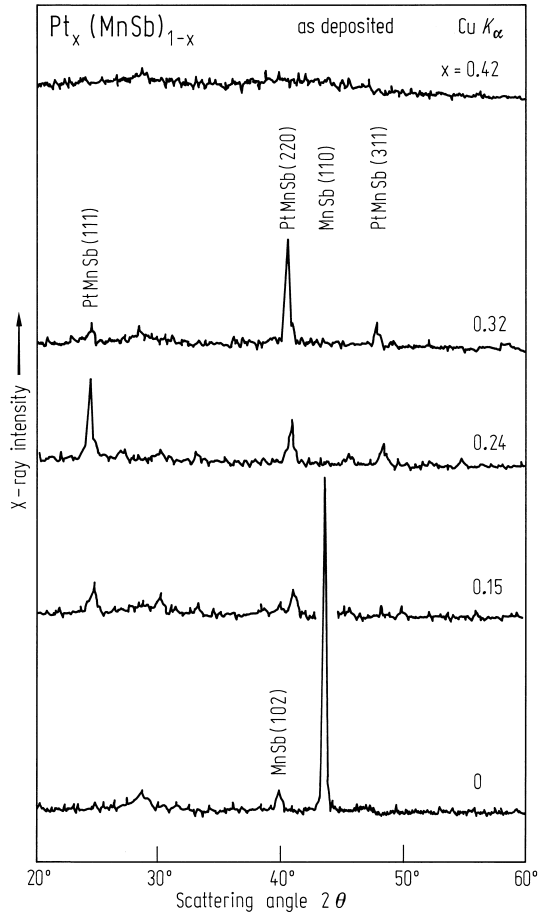

Fig. 650. X-ray diffraction patterns for as deposited $Pt_x(MnSb)_{1-x}$ ($0 \le x \le 0.42$) films at different values of x [87O1].

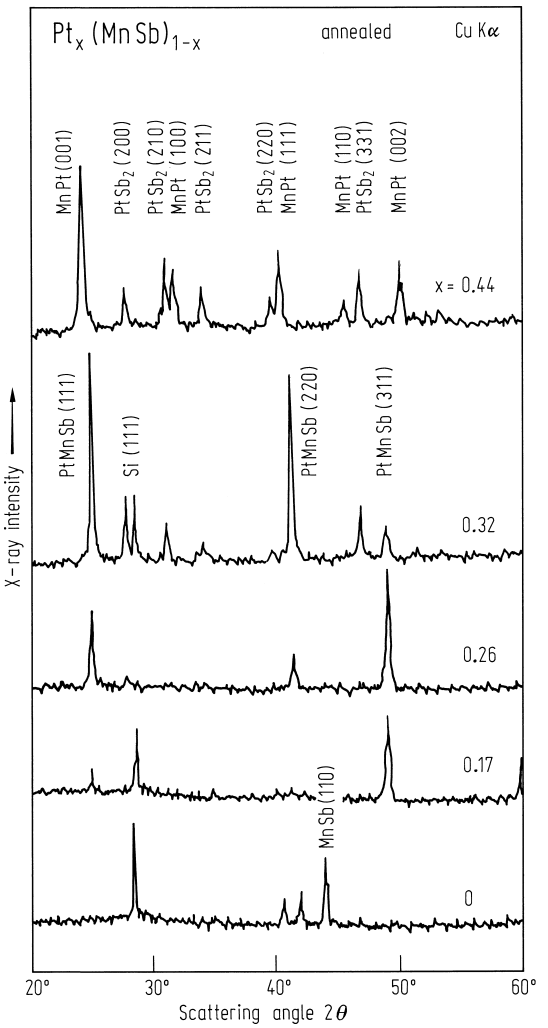

Fig. 651. X-ray diffraction patterns for annealed $Pt_x(MnSb)_{1-x}$ ($0 \le x \le 0.44$) films at different values of x [87O1].

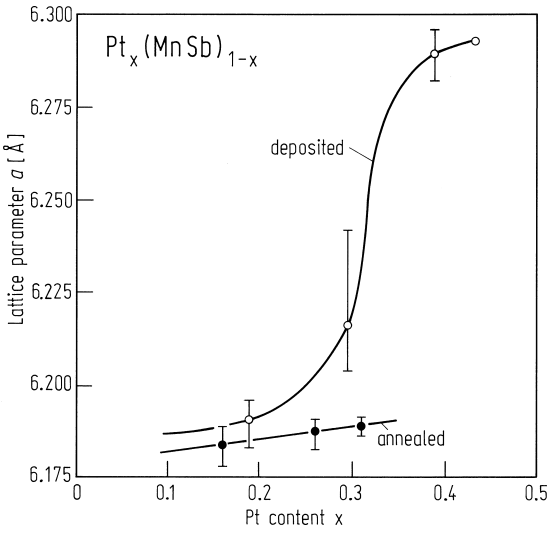

Fig. 652. Relationship between the Pt concentration in $Pt_x(MnSb)_{1-x}$ films and lattice constant *a* [87O1].

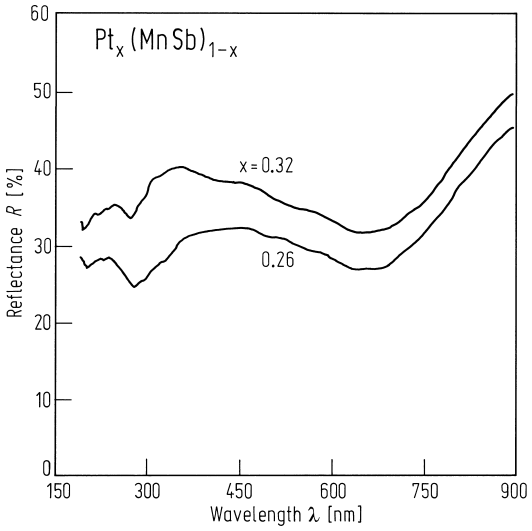

Fig. 653. Reflectance for annealed $Pt_x(MnSb)_{1-x}$ films of x = 0.32 and x = 0.26 in the wavelength range 190-900 nm [87O1].

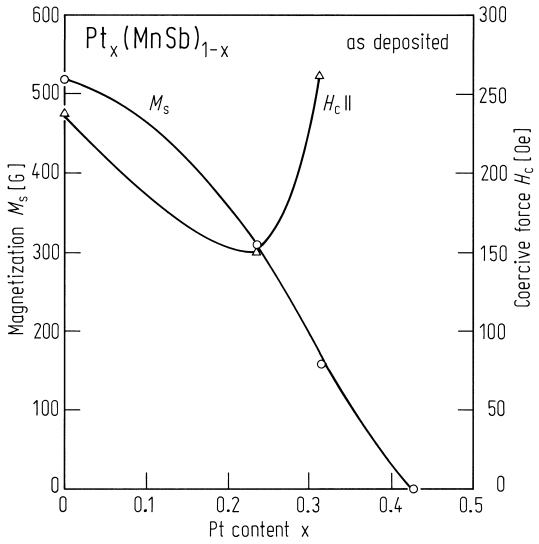

Fig. 655. Saturation magnetisation M_s and coercive force H_c in the film plane for as deposited $Pt_x(MnSb)_{1-x}$ films vs. Pt concentration [87O1].

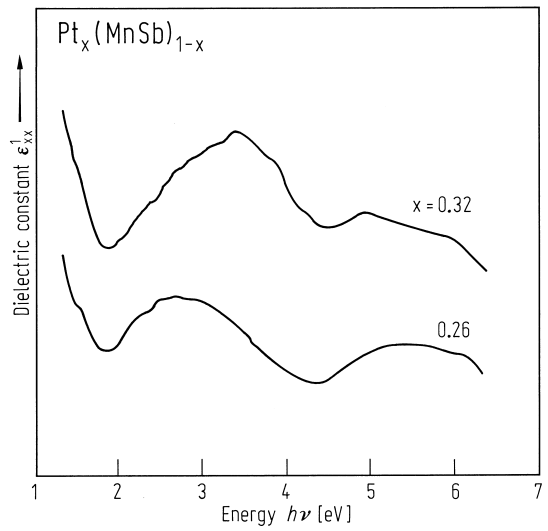

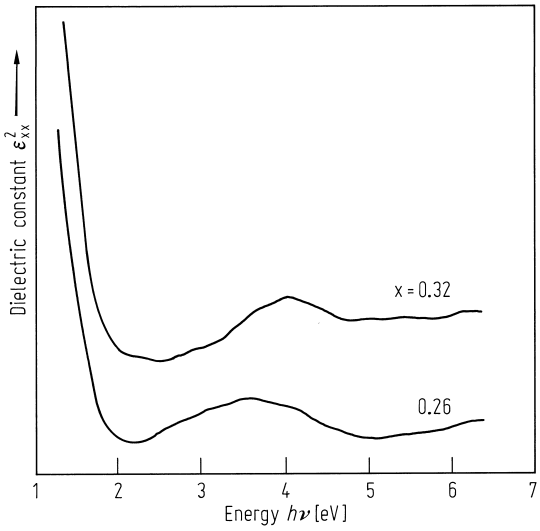

Fig. 654. Real (ε^1_{xx}) and imaginary (ε^2_{xx}) parts of the dielectric constants calculated using Kramers-Kronig relations from the reflection spectra for annealed $Pt_x(MnSb)_{1-x}$ films of x = 0.32 and x = 0.26 [87O1].

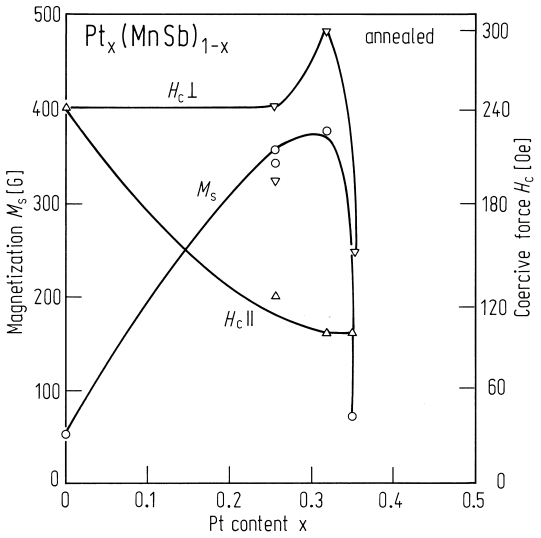

Fig. 656. Saturation magnetisation M_s and coercive force H_c parallel and perpendicular to the film plane for annealed $Pt_x(MnSb)_{1-x}$ films vs. Pt concentration [87O1].

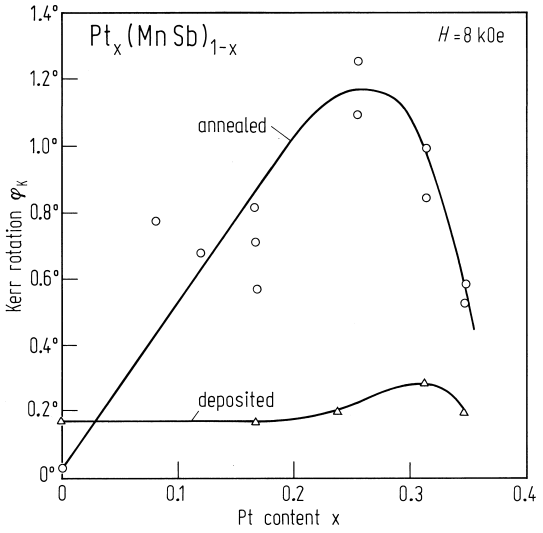

Fig. 657. Kerr rotation φ_K at room temperature for as-deposited and annealed $Pt_x(MnSb)_{1-x}$ films with different Pt concentrations, when an external magnetic field H = 8 kOe was applied perpendicular to the film plane (wavelength λ = 632.8 nm) [87O1].

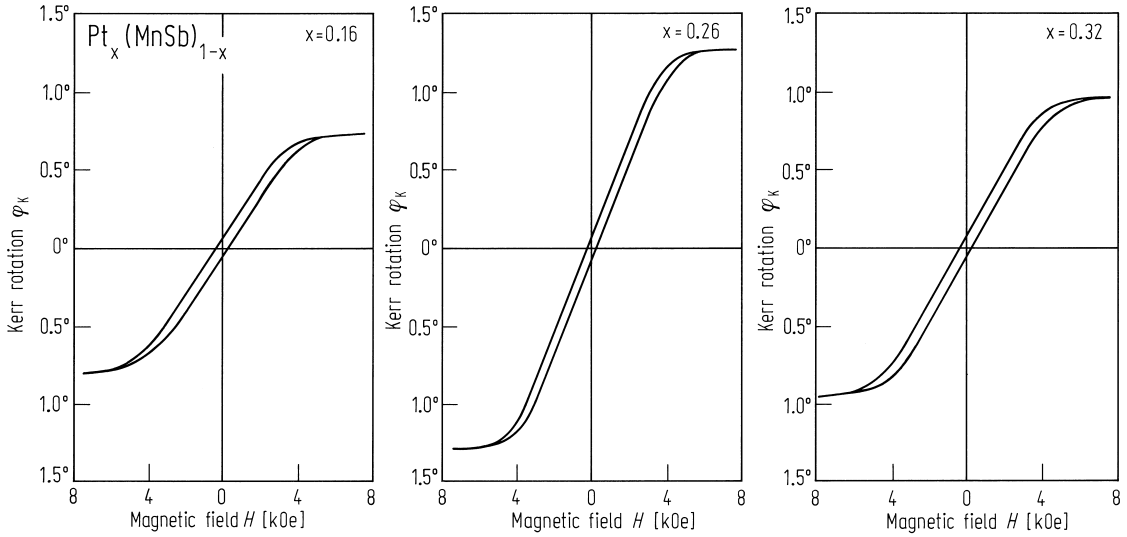

Fig. 658. φ_K-H hysteresis curves for the $Pt_x(MnSb)_{1-x}$ films of x = 0.16, 0.26 and 0.32 (wavelength λ = 632.8 nm) [87O1].

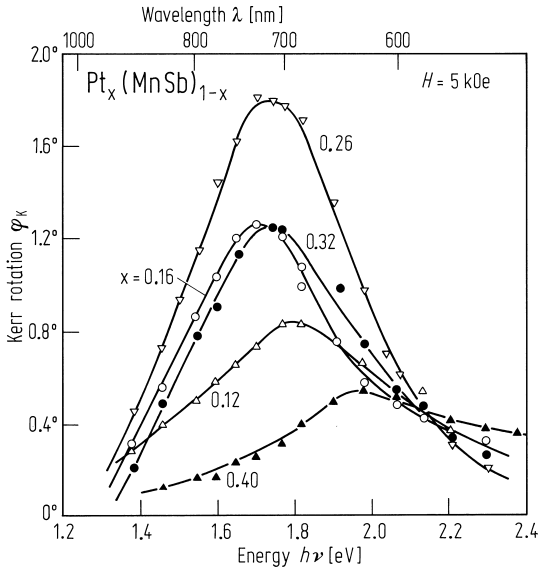

Fig. 659. Polar Kerr rotation φ_K spectra vs. wavelength for annealed $Pt_x(MnSb)_{1-x}$ films at different values of $0.16 \leq x \leq 0.42$) [87O1].

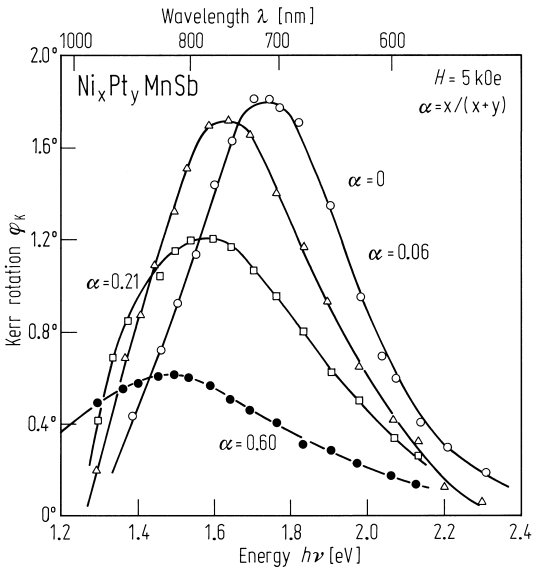

Fig. 660. Polar Kerr rotation φ_K spectra vs. wavelength for annealed Ni_xPt_yMnSb films with different ratios $\alpha = x/(x+y)$ [87O1].

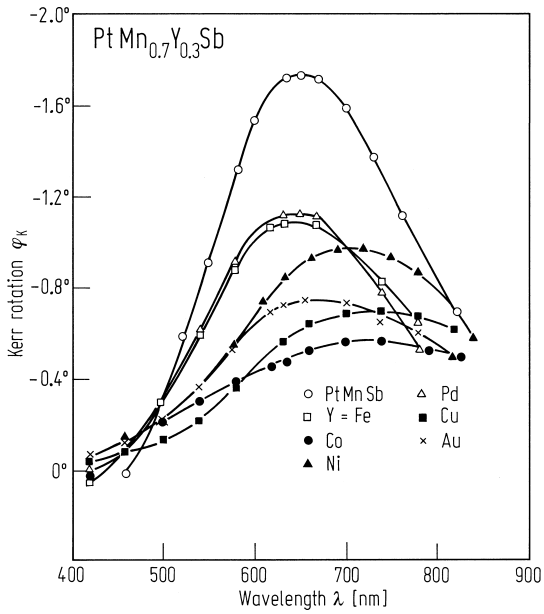

Fig. 661. Polar Kerr rotation vs. wavelength for $PtMn_{0.7}Y_{0.3}Sb$ thin films and a PtMnSb thin film [87I1].

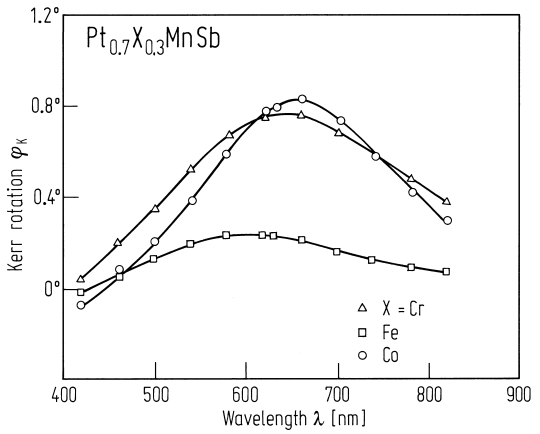

Fig. 662. Polar Kerr rotation vs. wavelength for $Pt_{0.7}X_{0.3}MnSb$ thin films [87I1].

Multilayers

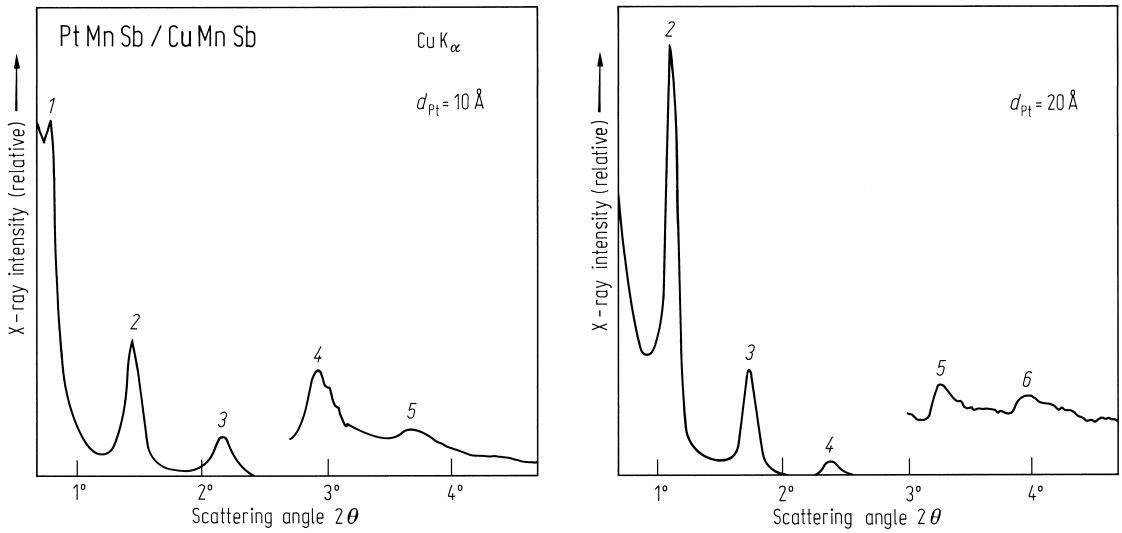

Fig. 663. Low angle X-ray diffraction patterns (CuK_α) for PtMnSb(d_{Pt})/CuMnSb(100Å) multilayer films [91W1].

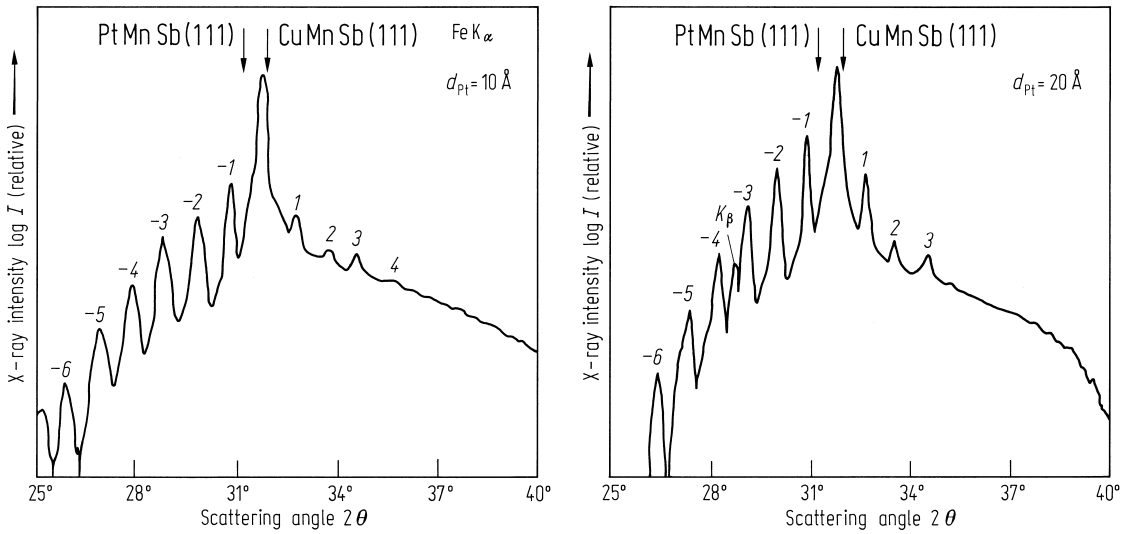

Fig. 664. Logarithm of the large angle X-ray diffraction pattern intensity (FeK_α) of PtMnSb(d_{Pt})/CuMnSb(100Å) multilayer films. The (111) peak positions of single-layer PtMnSb and CuMnSb films are indicated by arrows [91W1].

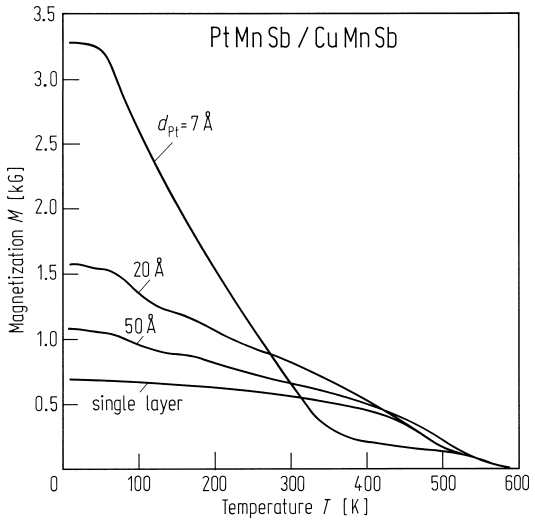

Fig. 665. Magnetisation as a function of temperature for PtMnSb(d_{Pt})/CuMnSb(100Å) multilayer films. The curve for a single layer PtMnSb film is shown for comparison [91W1].

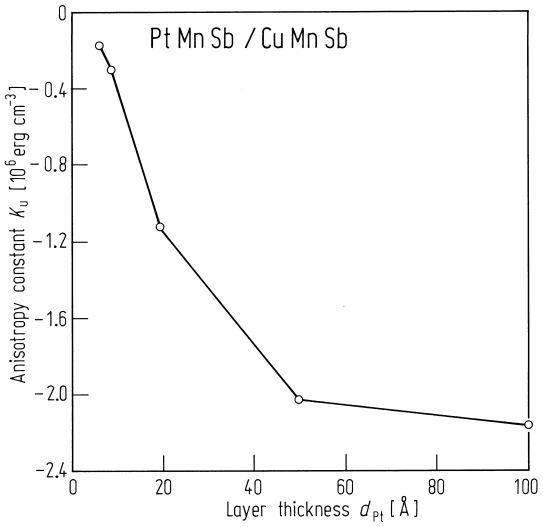

Fig. 666. d_{Pt} dependence of the uniaxial magnetic anisotropy constant K_u for PtMnSb(d_{Pt})/CuMnSb(100Å) multilayer films [91W1].

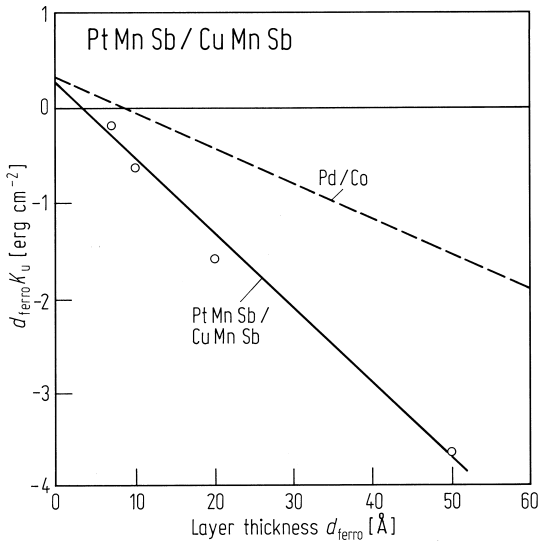

Fig. 667. d_{ferro} dependence of $d_{ferro}K_u$ for PtMnSb(d_{Pt})/CuMnSb(100Å) multilayer films where d_{ferro} is the thickness of each ferromagnetic layer. For comparison results for Pd/Co multilayer films are shown [91W1].

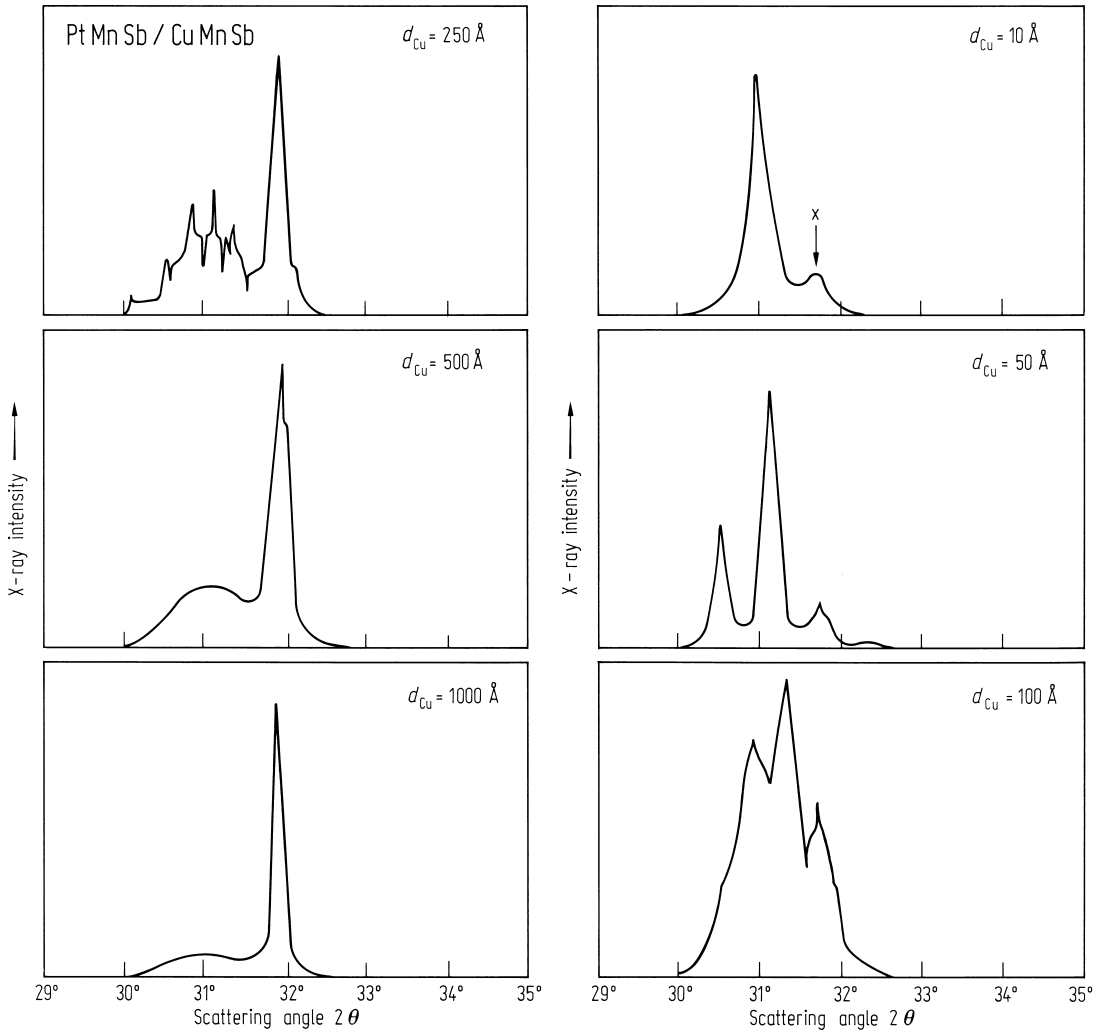

Fig. 668. X-ray diffraction patterns in the high angle region for PtMnSb(100Å)/CuMnSb(d_{Cu}) multilayer films. X in the case of d_{Cu} = 10 Å indicates the line due to the CuMnSb buffer layer [90T1].

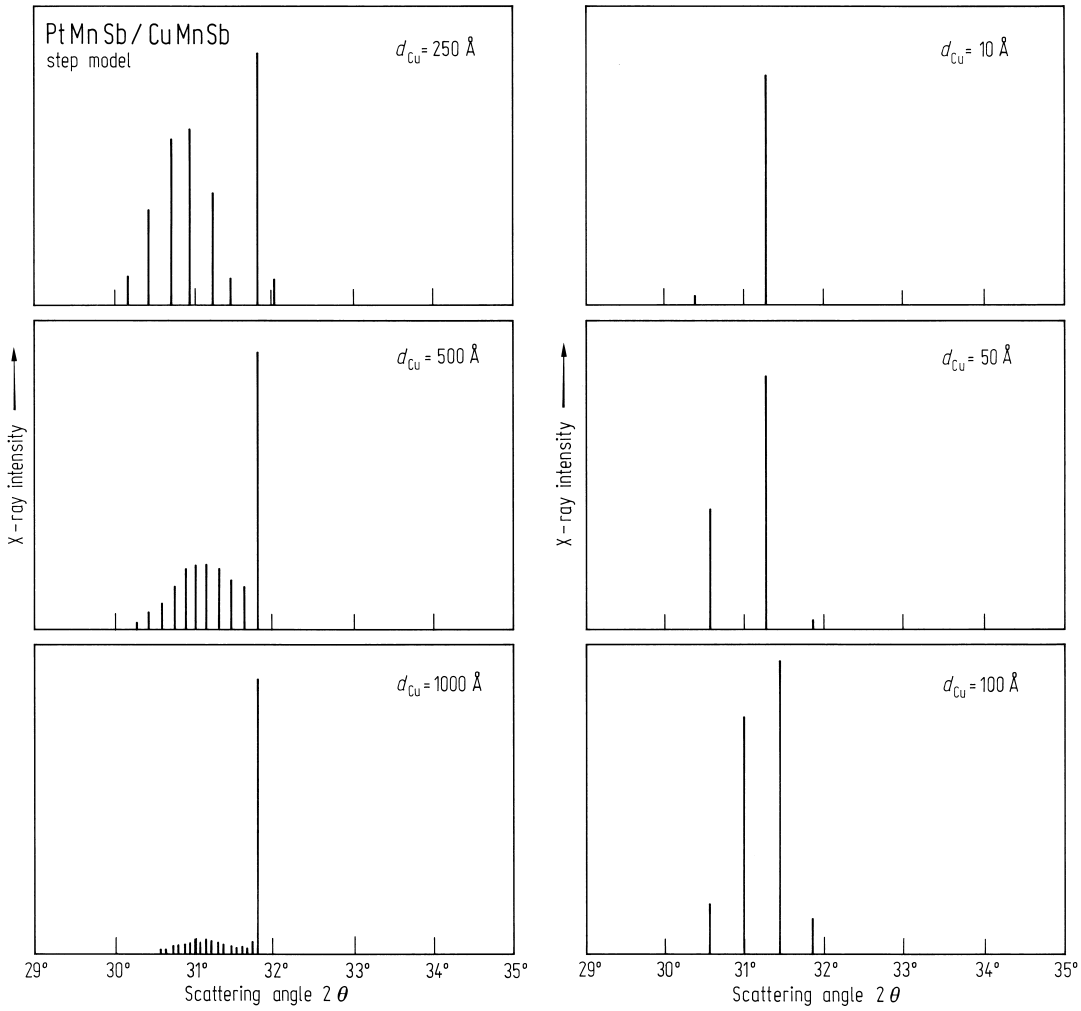

Fig. 669. Calculated X-ray diffraction patterns based on a step model for PtMnSb(100Å)/CuMnSb(d_{Cu}) multilayer films [90T1].

Table 132. Magnetisation values extrapolated to 0 K, $M(0)$, and Curie temperature T_C, for PtMnSb(d_{Pt})/CuMnSb(100Å) multilayer films. $M(0)$ is the value per unit volume of PtMnSb layers [91W1].

d_{Pt} [Å]	$M(0)$ [kG]	T_C [K]
3.6	4.4	248
7	3.1	307
10	2.2	369
20	1.6	485
50	1.1	524
100	0.82	500
single layer	0.67	525
bulk	0.65	582

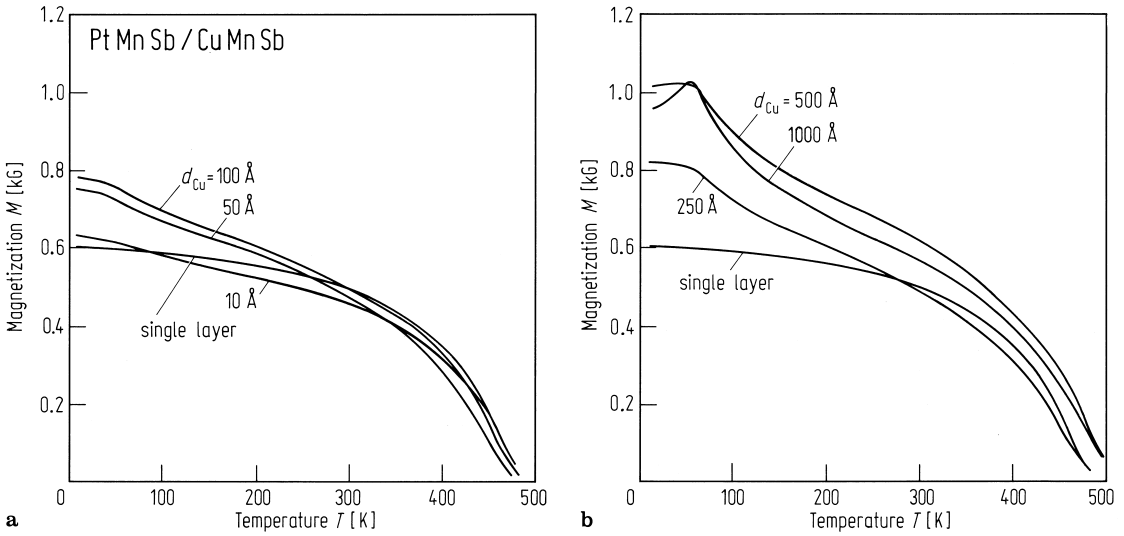

Fig. 670. *M-T* curves at the applied field of 0.3 T for PtMnSb(100Å)/CuMnSb(d_{Cu}) multilayer films [90T1]. (**a**) d_{Cu} = 10, 50, 100 Å, (**b**) d_{Cu} = 250, 500, 1000 Å. *M* is normalised by the volume of PtMnSb layers. The curve for a PtMnSb single layer film is also shown as a reference [90T1].

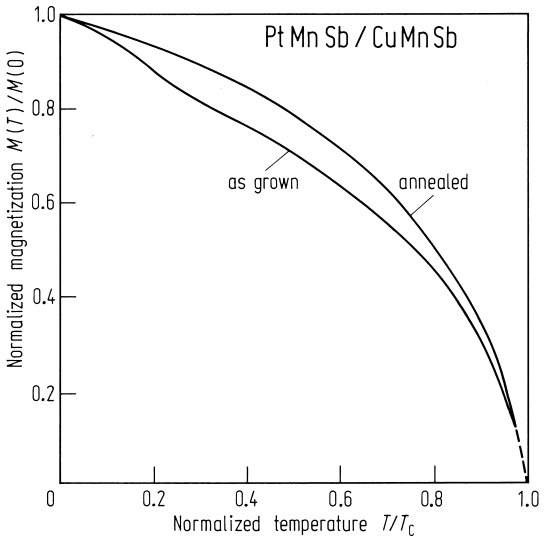

Fig. 671. $M(T)/M(0)$vs. T/T_C at an applied field of 0.3 T for PtMnSb(100Å)/CuMnSb(100Å) multilayer films as grown and annealed at 500 °C for 5 h [90T1].

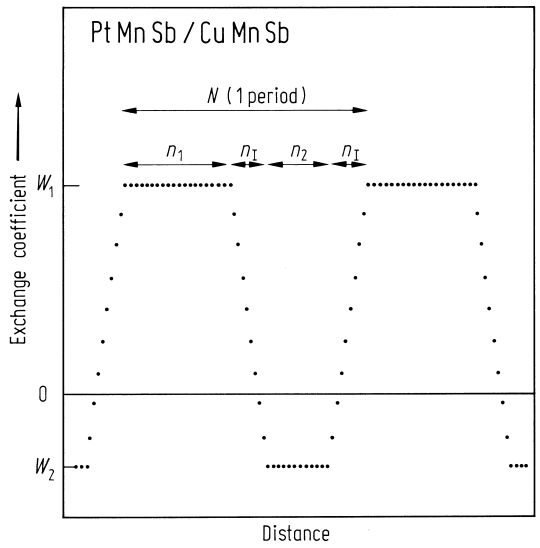

Fig. 672. Schematic diagram of the trapezoidal modulation of the exchange interaction. n_i denotes the number of atomic planes [90T1].

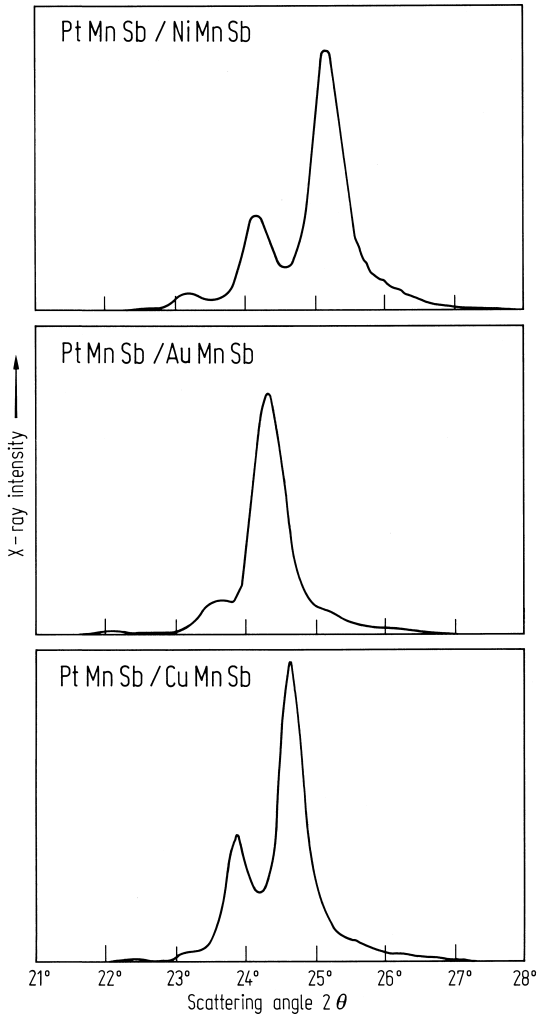

Fig. 674. X-ray diffraction patterns in the high angle region for PtMnSb/NiMnSb, PtMnSb/AuMnSb and PtMnSb/CuMnSb films with the multilayer period of 100 Å [89T1].

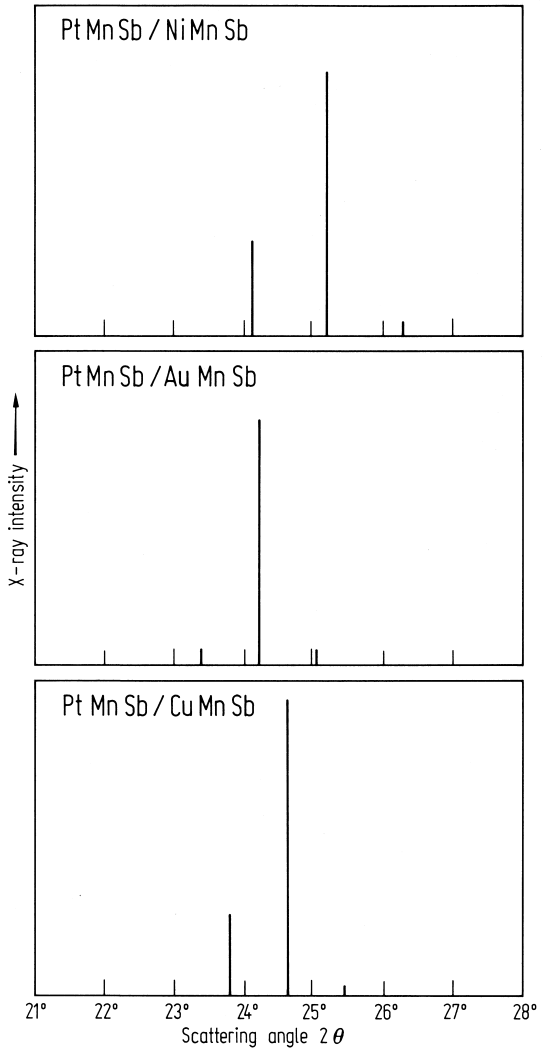

Fig. 675. Calculated X-ray diffraction patterns based on the step model for PtMnSb/NiMnSb, PtMnSb/AuMnSb and PtMnSb/CuMnSb films with the multilayer period of 100 Å [89T1].

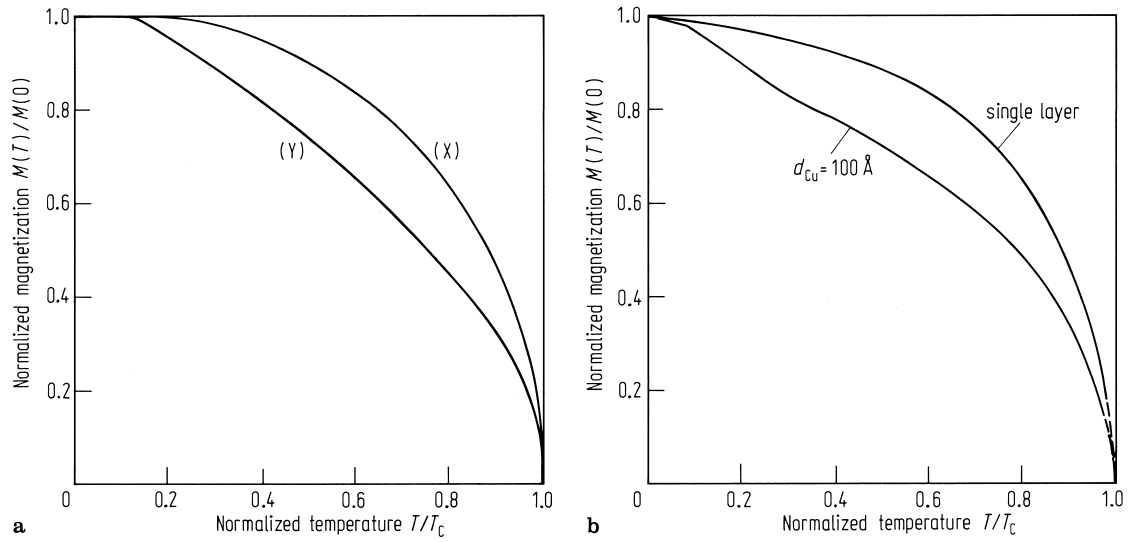

Fig. 673. Calculated $M/M(0)$ vs. T/T_C for multilayer samples. (X): N = 28, n_1 = 28, $n_2 = n_I$ = 0. (Y): N = 56, n_1 = 24, n_2 = 14, n_I = 9 [90T1].

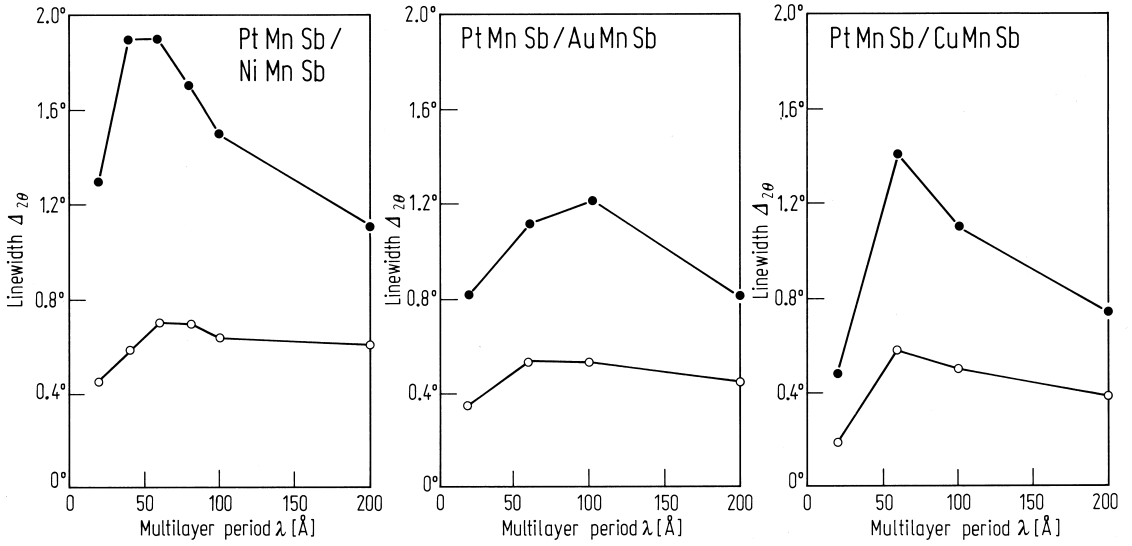

Fig. 676. X-ray diffraction linewidth $\Delta_{2\theta}$ for the (111) and (222) peaks (open and closed, respectively) vs. multilayer period λ for PtMnSb/NiMnSb, PtMnSb/AuMnSb and PtMnSb/CuMnSb films [89T1].

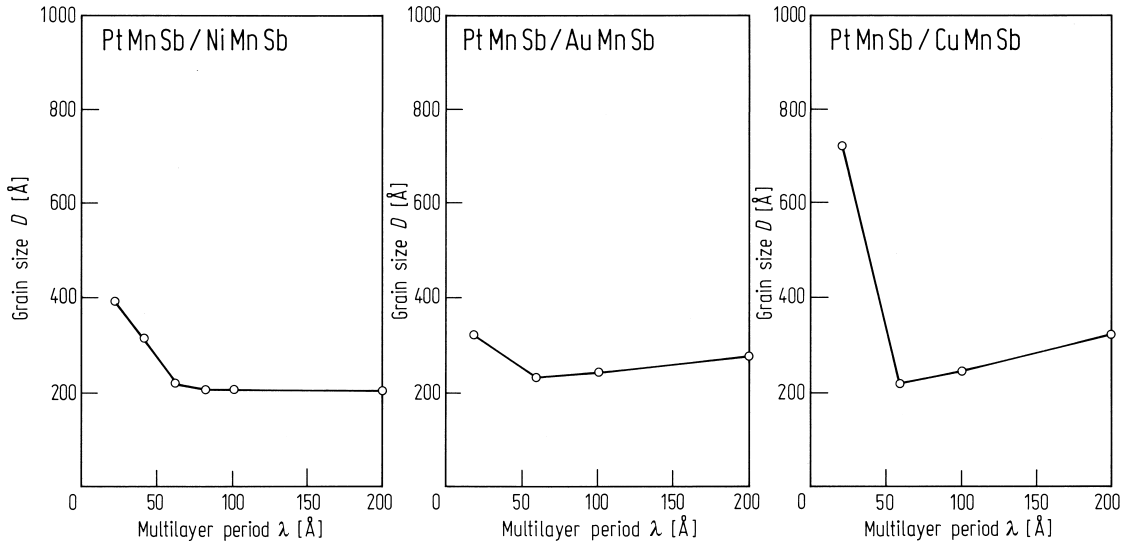

Fig. 677. Average grain size D vs. multilayer period λ for PtMnSb/NiMnSb, PtMnSb/AuMnSb and PtMnSb/CuMnSb films [89T1].

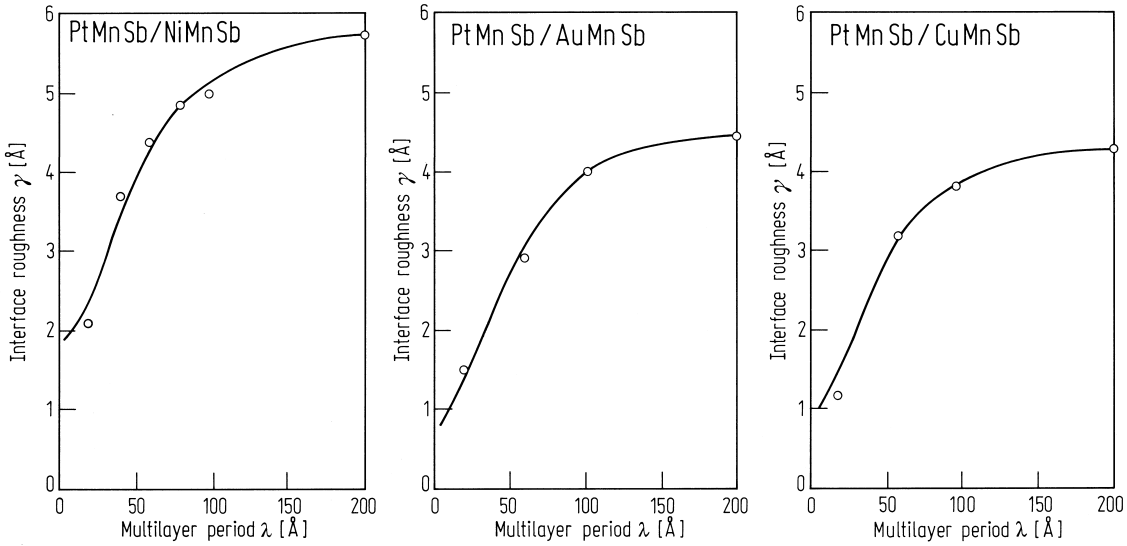

Fig. 678. Interface roughness γ vs. multilayer period λ for PtMnSb/NiMnSb, PtMnSb/AuMnSb and PtMnSb/CuMnSb films [89T1].

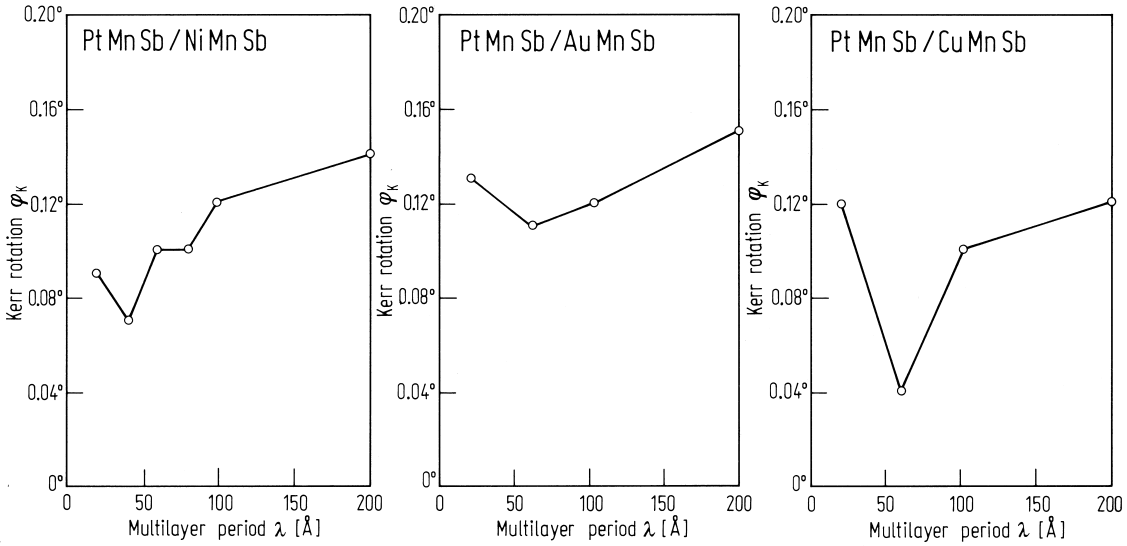

Fig. 679. Kerr rotation angle φ_K at a wavelength of 633 nm vs. multilayer period λ for PtMnSb/NiMnSb, PtMnSb/AuMnSb and PtMnSb/CuMnSb films [89T1].

1.5.5.12 References for 1.5.5

52S1 Stevens, K.W.H: Proc. Phys. Soc. A **65** (1952) 209.
56K1 Kasuya, T.: Prog. Theor. Phys. **16** (1956) 58.
57A1 Arrott, A.: Phys. Rev. **108** (1957) 1394.
61G1 Griffith, J.S.: The Theory of Transition Metal Ions C.U.P. (1961).
62L1 Lea, K.R., Leask, M.J., Wolf, W.P.: J. Phys. Chem. Solids **23** (1962) 1381.
63R1 Rhodes, P., Wohlfarth, E.P.: Proc. R. Soc. London A **273** (1963) 247.
68B1 Borovik-Romanov, S.: Magnetic Symmetry of Antiferromagnets; Elements of Theoretical Magnetism (Krupicka, S., Sternberk, J. Iliffe, eds.), (1968).
70K1 Khoi, L.D., Vijaraghawa, R., Malik, S.K., Nagrajan, V.: Phys. Lett. A **33** (1970) 435.
70S1 Shinohara, T.: J. Phys. Soc. Jpn. **28** (1970) 313.
73W1 Webster, P.J., Ziebeck, K.R.A.: J. Phys. Chem. Solids **32** (1973) 1647.
74Z1 Ziebeck, K.R.A., Webster, P.J.: J. Phys. Chem. Solids **35** (1974) 1.
75C1 Campbell, I.A., Blandin, A.: J. Magn. Magn. Mater. **1** (1975) 1.
75M1 Myers, H.P., Linder, L.: Phys. Scr. **12** (1975) 253.
75N1 Nikolaev, I.N., Potapov, V.P., Mar'in, V.P.: Sov. Phys. JETP **40** (1975) 591.
76C1 Kittel, C.: Introduction to Solid State Physics, New York: John Wiley Sons (1976).
76S1 Switendick, A.C.: Solid State Commun. **19** (1976) 511.
76Z1 Ziebeck, K.R.A., Webster, P.J.: Philos. Mag. **34** (1976) 973.
78L1 LeDang, K., Veillet, P., Campbell, I.A.: J. Phys. F **8** (1978) (1811).
78P1 Price, D.C.: J. Phys. F **8** (1978) 933.
78Y1 Yagasaki, K., Hidaka, Y., Fujii, H. Okamoto, T.: J. Phys. Soc. Jpn. **45** (1978) 110.
79B1 Bronstein, I.N., Semendjajew, K.A.: Taschenbuch der Mathematik, Frankfurt/Main: Harri Deutsch (1979).
79F1 Freemann, A.J., Desclaux, J.P.: J. Magn. Magn. Mater. **12** (1979) 22.
79M1 Mager, S., Wieser, E., Zemcik, T., Schneeweiss, O., Stetsenko, P.N., Surikov, V.V.: Phys. Status Solidi (a) **52** (1979) 249.
79W1 Webster, P.J., Ramadan, M.R.I.: J. Magn. Magn. Mater. **13** (1979) 301.